Human cytokine receptor CRLF3 is a receptor for the neuroprotective erythropoietin splice variant EV-3

Debbra Y Knorr
Göttingen University https://orcid.org/0000-0002-3334-0330
Ignacio Rodriguez Polo
German Primate Center https://orcid.org/0000-0003-1254-4972
Hanna S Pies
Göttingen university
Nicola Schwedhelm-Domeyer
Göttingen University
Stephanie Pauls
Göttingen University
Rüdiger Behr
German Primate Center
Ralf Heinrich (rheinri1@gwdg.de)
Göttingen University https://orcid.org/0000-0002-8369-0507

Research Article

Keywords: CRLF3, Cytokine receptor, Cytoprotection, Neuroprotection, Erythropoietin, EV-3

Posted Date: August 3rd, 2022

DOI: https://doi.org/10.21203/rs.3.rs-1917090/v1

Abstract

Cytokine receptor like factor 3 (CRLF3) is a conserved cytokine receptor present in all major eumetazoan taxa. Though vertebrate CRLF3 has recently been implied in the regulation of hematopoiesis, its ligand remained unidentified. CRLF3 shares structural similarity with receptors for other hematopoietic growth factors including erythropoietin, thrombopoietin and granulocyte colony-stimulating factor. Besides hematopoietic organs, these established hematopoietic cytokines and their receptors are also widely expressed in other tissues including the nervous system, where they regulate proliferation, differentiation, cell survival and other homeostatic processes. Previous studies identified insect CRLF3 as a neuroprotective receptor that can be activated by human recombinant erythropoietin, a widely accepted protective cytokine in vertebrate nervous systems. Epo's erythropoietic functions mediated by classical Epo receptor are understood in great detail whereas Epo-mediated cytoprotective mechanisms are more complex due to involvement of additional Epo receptors and a splice variant (EV-3) with selectivity for certain unidentified receptors. In the present study, we show that human CRLF3 mediates neuroprotection upon activation with the natural Epo splice variant EV-3. We generated *CRLF3* knock out iPSC lines and differentiated them towards the neuronal lineage. While apoptotic death of rotenone-challenged wild type iPSC-derived neurons was prevented by EV-3, EV-3-mediated neuroprotection was absent in *CRLF3* knock out neurons. Rotenone-induced apoptosis and EV-3-mediated neuroprotection were associated with differential expression of pro- and anti-apoptotic genes. Our data characterize human CRLF3 as a receptor involved in Epo-mediated neuroprotection and identify CRLF3 as the first known receptor for EV-3.

Introduction

Various hematopoietic growth factors that regulate the production of blood cells mediate additional homeostatic functions in other non-hematopoietic tissues. Examples are erythropoietin (Epo), thrombopoietin (Tpo) and granulocyte colony-stimulating factor (GCSF), all of which are also expressed in mammalian nervous systems where they regulate development, differentiation and cell survival [1–4]. Their receptors (EpoR, TpoR and GCSFR) belong to the class I family of cytokine type I receptors that possess the extracellular cytokine receptor homology domain and an WSXWS motif [5–7]. Another member of this hematopoietic cytokine receptor family is the orphan cytokine receptor-like factor 3 (CRLF3) which was recently implicated in zebrafish hematopoiesis [8] and mammalian thrombopoiesis [9]. Human CRLF3 contains the characteristic cytokine receptor motif (WSXWS), a single-pass transmembrane region and a Janus kinase docking site and is expressed in various tissues including the nervous system [5, 10]. Though its ligand has not been identified and signalling mechanisms are largely unknown, CRLF3 has been associated with the regulation of proliferation, differentiation and cell survival [11, 12] similar to its structurally related receptors for other hematopoietic cytokines. Moreover, CRLF3 levels have been detected in tumours and various tumour cell lines [13, 14] and sequence alterations have been linked to amyotrophic lateral sclerosis (ALS) [15], autism spectrum disorders [11] and sensitivity to *Leishmania* infections [16]. In contrast to the vertebrate-specific

members of its cytokine receptor family, CRLF3 is highly conserved and present in all major eumetazoan taxa including cnidarians, various invertebrates and vertebrates including humans [5–8]. Previous studies on locusts and beetles reported that the insect ortholog of CRLF3 mediates potent neuroprotection upon stimulation with human recombinant Epo [6, 10].

The vertebrate-specific helical cytokine erythropoietin (Epo) is a major kidney-derived hormonal regulator of hematopoiesis, that protects erythroid progenitor cells from apoptosis to promote increased numbers of oxygen-transporting mature erythrocytes [17–19]. Local expression and release of Epo has been described for various tissues including brain, liver and lung and numerous studies reported its cytoprotective and regenerative functions in these and other tissues (reviewed in [20–22]). With respect to the nervous system, Epo is crucial for normal brain development, acts neuroprotectively after hypoxic/ischemic and other toxic insults and promotes regeneration after axonal damage [23–26]. Beneficial functions also included enhanced cognitive performance and memory functions in healthy humans and patients affected by schizophrenia and mood disorders [27–30]. Clinical studies explored the potential of Epo to interfere with cell loss in neurodegenerative diseases including Alzheimer's disease, Parkinson's disease and amyotrophic lateral sclerosis [31–33]. A drawback of prolonged and/or high dose Epo administration is the overproduction of erythrocytes leading to increased risk of thrombosis, stimulation of cancerogenic cell proliferation and tumor vascularization all resulting from activation of homodimeric classical EpoR [34–37]. Studies with Epo-mimetics (some with partial sequence similarity, others with rather unrelated structure compared to full Epo) have demonstrated neuroprotective and regenerative effects without activation of homodimeric EpoR [38–41]. Some of these may activate a heteroreceptor consisting of EpoR and b common receptor (synonym CD131), which mediates neuroprotection in some but not all brain regions [42–47]. The naturally occurring Epo splice variant EV-3, characterized by the lack of exon 3, mediates neuroprotection independent of both homodimeric and heteromeric EpoR suggesting that additional alternative neuroprotective receptors for Epo-like signals exist in the mammalian brain [48, 49].

Studies on insects demonstrated that both, human recombinant Epo and EV-3 increased the survival of hypoxia- or toxin-challenged neurons by activation of cytokine receptor-like factor 3 (CRLF3) [6, 10, 50, 51] suggesting that CRLF3 might be a general neuro- or tissue-protective receptor for Epo-like cytokines across species. CRLF3 shares both structural similarity and regulatory roles in blood cell production with EpoR, TpoR and GCSFR [5, 7–9]. All of these receptors are also expressed in vertebrate nervous systems but, in contrast to EpoR, TpoR and GCSFR, neither the activating ligand nor a concrete function of CRLF3 in non-hematopoietic tissue were so far identified.

In light of highly conserved *CRLF3* orthologues in insects and mammals, we hypothesized that Epo mediates cell-protective functions via activation of CRLF3 in human neurons, as it was previously reported for insect CRLF3. To study whether Epo/CRLF3-signalling protects human neurons from stress-induced apoptosis we established survival assays with human induced pluripotent stem cell- derived neurons.

Induced pluripotent stem cells (iPSC), that can give rise to various cell types upon exposure to appropriate differentiation protocols, harbour great potential for biomedical research and disease modelling [52–55]. We generated *CRLF3* knock out (KO) iPSC lines along with isogenic control lines (Ig-Ctrl) from two independent human iPSC lines by means of a Piggy-Bac-CRISPR-Cas9 system and differentiated them into neuron-like cells. Apoptosis was induced through “chemical hypoxia” by addition of rotenone, an inhibitor of complex I of the mitochondrial electron transport chain. CRLF3 was stimulated with the natural human Epo splice variant EV-3 to prevent coactivation of homodimeric EpoR or EpoR/ βcR [48]. We demonstrate that EV-3 protects WT and Ig-Ctrl iPSC-derived neurons from rotenone-induced apoptosis. In contrast, *CRLF3*-KO neurons were not protected, indicating that CRLF3 serves as neuroprotective receptor for EV-3 in human neurons. The results of our study deorphanize human CRLF3 by identifying EV-3 (and most likely also Epo) as a natural ligand. Moreover, we show that EV-3/CRLF3 signalling mediates protection of human cells indicating that CRLF3 can be selectively targeted by Epo-like ligands to counteract neurodegenerative diseases without simultaneously promoting inappropriate erythropoiesis and tumor growth.

Methods

Experiments were conducted with two human iPSC lines. iPSC were generated from commercially available human fibroblasts originating from a female and a male patient (referred to from now as iPSC#1 and iPSC#2 respectively; Lonza CC-2511, lot 0000490824 [iPSC#1], and lot 0000545147 [iPSC#2]). Reprogramming was performed according to Okita et al. [70]. iPSC characterization was described in Stauske et al. [71]. Human iPSC were maintained at 37°C, 5% CO_2 in Universal primate pluripotent stem cell medium (UPPS medium), and cell splitting was performed using Versene solution (Thermo Fisher Scientific; #15040066) according to Stauske et al. [71]. iPSC were cultured on Geltrex-coated 6 cm or 12- well dishes (Thermo Fisher; A1413202). For all molecular analysis described below, cells (both iPSC and iPSC-derived neurons) were washed twice in Phosphate buffered saline (PBS) before being scraped (Cell scraper, Sarstedt; #833945040) and collected in an 1,5 ml Eppendorf tube. Cell suspensions were centrifuged at 12.000 x g for 2 min. PBS was removed and cell pellets snap-frozen in liquid nitrogen. Samples were stored at -80°C until further analysis.

Establishment and characterization of transgenic lines

The KO lines were generated according to Rodríguez-Polo et al. [56], following a constitutive Cas9-gRNA expression strategy. In brief, cells were nucleofected with a piggyBac-CRISPR-Cas9-GFP vector carrying a guide RNA (gRNA) specifically targeting *CRLF3* (see Table 1) and a second vector carrying Transposase-dtTomato, (Pac-PB-Tomato) [57]. In parallel, a different subset of cells was transfected with an empty piggyBac-CRISPR-Cas9 (no gRNA) construct in order to generate isogenic control (Ig-Ctrl) lines. After transfection the GFP positive (Cas9-GFP-gRNA positive) population was sorted by Fluorescence assisted cell sorting (FACS; Sony Flow Cytometry FACS SH800S). The presence of INDEL mutations in the

polyclonal population was evaluated using PCR (Primer sequences see Table 1) in combination with T7 endonuclease I assay and Sanger sequencing. For the generation of the CRLF3 KO monoclonal lines, polyclonal populations were single-cell sorted into a 96-well plate, expanded and genotyped. Presence of the transgene was evaluated by GFP expression using a Zeiss Observer Fluorescent microscope (Carl Zeiss, #4001584). Successful introduction of loss-of-function mutations was evaluated in the monoclonal lines amplifying the targeted locus by PCR, subcloning the product in pCRII vector (TA cloning kit; Thermo Fisher Scientific # K207020), transforming the vector into competent *E.coli*, and sequencing by Sanger (20 bacterial clones per cell line analysed). Subsequent sequence analysis revealed allele-specific variations in each one of the iPSC clones. Additionally, protein depletion from mutated iPSC and iPSC-neurons was confirmed by Western blot (see below).

Genomic DNA extraction and PCR

Genomic DNA (gDNA) was extracted using DNeasy Blood & Tissue Kit (Qiagen; #69504) according to the manufacturer's instructions. The gRNA target site was amplified using specific primers as stated below (Table 1). PCR was run using GoTaq Green Master Mix (Promega; #M7122) and PCR program was set as shown in Table 2. PCR products were loaded on a 1% agarose gel and run for 30 min at 100 V before extracting DNA fragments using Macherey–Nagel NucleoSpin Gel and PCR Clean-up Kit (Macherey–Nagel; #740609.50). The isolated DNA fragments were subsequently either sent for sequencing using specific PCR primers (for Polyclonal approach; Sequencing facility Microsynth AG, Göttingen, Germany) or cloned into a pCRII vector for allele characterization (for clonal expansion).

Table 1: Oligonucleotides

Application	Gene	Oligonucleotide 5'-3'	Tm	Accession number
gRNA	CRLF3-fwd	CACCGAAAGGCCTCGCACATTCAGT		ENSP00000318804.6
gRNA	CRLF3-rev	AAACACTGAATGTGCGAGGCCTTTC		
PCR	CRLF3-fwd	CCCTGGGCTTTCTGCTTTGC	61°C	
PCR	CRLF3-rev	ACCACGCATGGTCTGAAAACC		
qPCR	CRLF3 fwd	CAACGTTGGGGTCTATGTGC	61°C	
qPCR	CRLF3 rev	CGCCCACCAGTACAGATAGA		
qPCR	Bax- fwd	CGAGTGGCAGCTGACATGTT	61°C	ENST00000293288.12
qPCR	Bax- rev	TCCAGCCCATGATGGTTCTG		
qPCR	Caspase 3-fwd	GGAGGCCGACTTCTTGTATG	61°C	ENST00000308394.9
qPCR	Caspase 3-rev	TGCCACCTTTCGGTTAACCC		
qPCR	BCL-2-fwd	CGTTATCCTGGATCCAGGTG	61°C	ENST00000398117.1
qPCR	BCL-2- rev	GTGTGTGGAGAGCGTCAAC		
qPCR	bActin-fwd	GCGAGAAGATGACCCAGATC	61°C	ENST00000674681.1
qPCR	bActin- rev	GGGCATACCCCTCGTAGATG		

Table 2: PCR program for CRLF3 amplification

Step	Temperature [°C]	Time [sec]	Cycle
Initial denaturation	95	180	
Denaturation	95	30	x30
Annealing	61	30	
Elongation	72	30	
Final elongation	72	300	

Transformation

pCRII vectors carrying PCR products of single-cell clones were transformed into XL1-blue competent cells (Agilent; #200249). 500 ng plasmid were carefully mixed with 100 µl of competent cells and let to rest on ice for 30 min. Subsequently, cells received a heat shock at 42°C for 40 sec before 900 µl super optimal broth (SOB) (Roth; #AE27.1) without antibiotics was added. Cell suspension was transferred into a bacterial incubator for 1 h at 37°C, 225 rpm. Afterwards, cell suspension was centrifuged at 3000 x g for 2 min, supernatant was removed, and cells were resuspended in 100 ml SOB medium before being dispersed on LB agar plates + ampicillin (Sigma-Aldrich; #L2897). Plates were let to rest at room temperature (RT) for 10 min before being transferred to 37°C.

Western blot

Cell pellets were lysed in protein lysis buffer (150mM NaCL; 20mM Tris.HCl pH 7.5; 1mM EDTA; 1% Triton-X-100) + Protease inhibitor (Thermo Fisher Scientific; #78429) by vigorous shaking in a tissue lyser (Qiagen; #85300) for 3 min at 50 Hz. Subsequently, the lysates were transferred onto ice and incubated for 30 min. Cell lysate was centrifuged at 10.000 x g for 10 min at 4°C and the protein containing supernatant was transferred to a fresh Eppendorf tube. Protein concentration was measured by Bradford assay (PanReac AppliChem; #A6932,0500). For all Western blots run in this study 50 µg protein was denatured in 2X Lämmli buffer (Sigma-Aldrich; #S3401) at 95°C for 5 min. 10% SDS-Pages were run for 30 min at 70 V and 1 h at 120 V. For size reference, PageRuler Plus Prestained Protein ladder (Thermo Fisher Scientific; #26619) was loaded together with samples. The separated protein was transferred onto nitrocellulose membranes (Roth; #9200.1) in a wet blot approach for 1,5 h at 180 mA. Membranes were incubated in Ponceau S (Sigma-Aldrich; #P3504) in order to check for sufficient and successful protein transfer before being blocked in 5% Milk/ PBS-0,1% Tween-20 (PBST) for 30 min at room temperature (Milk Roth; #T145; Tween-20 PanReac AppliChem; #A7564). Membranes were probed for CRLF3 (see antibody list for dilutions in table 3) either at RT for 2 h or overnight at 4°C. Subsequently, membranes were washed 3 times in PBST before incubation in α-HRP solution for 30 min at RT. Membranes were imaged by incubation in Pierce ECL Western blotting substrate (Thermo Fisher Scientific; #32209) using iBright CL1500 Imaging System (Thermo Fisher Scientific; **#**A44114). Subsequently, membranes were stripped in 0,5 M NaOH for 3 min, washed 3 times in PBS before being blocked again. Membranes were incubated in αTubulin (see table 3) for 1 h at RT before incubation with the secondary α-HRP antibody and imaging. Quantification of protein band intensities was performed using ImageJ. Band intensities were normalized to the corresponding αTubulin band intensity of each sample and then towards control samples within treatment groups. Data is shown as bar plots representing the average band intensities measured together with the calculated standard deviation and single data points.

Transgenic iPSC characterization

To confirm pluripotency of the newly generated transgenic lines (namely CRLF3 KO and corresponding Ig Ctrl of iPSC#1 and #2) we stained for pluripotency markers NANOG and OCT4A (see antibody list in table 3). iPSC were grown on 2 cm glass coverslips (Menzel-Gläser, #CB00200RA1) and fixed when confluent in 4% Paraformaldehyde (PFA) for 30 min. Coverslips were subsequently washed 3x in PBS before being blocked in 0,5 % bovine serum albumin (BSA; Thermo Fisher Scientific, #15260037) either for 30 min at RT or longer at 4°C. Cells were washed again 3 times in PBS and subsequently incubated with primary antibody according to table 3 at 4°C overnight. Coverslips were washed 3 times in PBS before incubation with the corresponding secondary antibody (table 3) at 37°C for 1 h. Cells were washed three times in PBS and once in water before mounting in Fluoromount-G (Thermo Fisher Scientific, #00-4958-02). Images were taken with a Zeiss Observer Fluorescent microscope.

To show that differentiation capacities of transgenic lines remain intact after transgenesis we performed spontaneous differentiation assays, by embryoid body formation (EB), according to Rodriguez-Polo *et al.*, [52]. In brief, iPSC colonies were detached with 200 U/ml Collagenase Type IV for 10 min at 37°C, scraped off and transferred to uncoated bacterial dishes. EBs were maintained in Iscoves medium (Thermo Fisher Scientific, # 12440053) at 37°C and the medium changed every second day.

After 8 days EB were transferred onto Geltrex-coated 6-well plates equipped with 2 cm coverslips for spontaneous differentiation and further maintained in Iscove's Medium. Cells were fixed between day 18 and 20. Stainings were performed as described above. Spontaneously differentiated cells were stained for Smooth muscle actin (SMA) and α-Fetoprotein according to table 3.

*Table 3: **Antibodies used***

Antibody	Company	Host	Dilution	Application
CRLF3	Santa Cruz; #sc-398388	mouse	1:500	IF / Western blot
αTubulin	Sigma-Aldrich; T9026	mouse	1:5000	Western blot
Nanog	Cell Signaling, #D73G4	rabbit	1:400	IF
OCT4A	Cell Signaling, #C53G3	rabbit	1:1600	IF
SMA	Sigma-Aldrich, #A2547	mouse	1:100	IF
αFetoprotein	Dako, #A0008	rabbit	1:100	IF
Neurofilament 200	Sigma-Aldrich; #N4142	rabbit	1:400	IF
ß-III-tubulin/AF 594	Santa Cruz; #sc-80005 AF594	mouse	1:50	IF / FACS
Phantom dye red 780	Proteintech; #PD00002	/	1:1000	FACS
Alexa Fluor 555	Thermo Fisher; #A32727	mouse	1:1000	IF
Alexa Fluor 594	Thermo Fisher; #A32732	rabbit	1:1000	IF
Alexa Fluor 633	Thermo Fisher; #A21070	rabbit	1:1000	IF
HRP	Sigma-Aldrich; #A4416	mouse	1:10000	Western blot

Neuronal differentiation and survival-assay establishment

iPSC were differentiated as described previously [58] with slight modifications of the original protocol. iPSC were split on 12-well plates and maintained in UPPS until reaching confluency of 60-80%. Medium was changed every 2nd to 3rd day. For the first 7 days of differentiation, cells were maintained in induction medium consisting of DMEM/F12 (Thermo Fisher Scientific; #11320033), 10% Knock out serum (KOS; Thermo Fisher Scientific; # 10828028), 1% Non-essential amino acids (NEAA, Thermo Fisher Scientific;# 11140050), 200 µM L-Ascorbic Acid (L-AA, Sigma-Aldrich; # A92902-100G), 2 µM SB431542 (Peprotech; # 3014193), 3 µM Chir99021 (Sigma-Aldrich, # SML1046) and 1,5 µM dorsomorphin (Peprotech, # 8666430). Cells were split onto fresh Geltrex-coated plates on day 6. Neuron splitting was performed following incubation in 0,25% Trypsin/EDTA (Thermo Fisher Scientific; # 25200056) for 3 min at 37°C. Cells were scraped and carefully resuspended before collection in a 5 ml falcon containing 5 ml DMEM/FBS. Cell suspension was centrifuged for 5 min at 200 x g. The supernatant was discarded, cells were resuspended in Induction medium + 0,001 % ß-mercaptoethanol (Thermo Fisher Scientific;

#21985023) and seeded onto 6-well plates. Medium was changed the next day to neuralization medium containing DMEM/F12, 200 µM L-AA, 1% NEAA, 1X N2 supplement (Thermo Fisher Scientific; # 17502048), 1X B27 supplement (Thermo Fisher Scientific; #17504044), 10 ng/ml bFGF (Peprotech; #100-18B) and 10 ng/ml EGF (Peprotech; #AF-100-15). Cells were fed with neuralization medium for one week before switching to neuronal differentiation medium I, consisting of DMEM/F12, 200 µM L-AA, 1% NEAA, 1X N2 supplement, 1X B27 supplement, 300 ng/ml cAMP (Peprotech; #6099240). For the final 7 days of neural differentiation, cells were maintained in neural differentiation medium II containing DMEM/F12, 200 µM L-AA, 1% NEAA, 1X N2 supplement, 1X B27 supplement, 300 ng/ml cAMP, 10 ng/ml BDNF (Peprotech; #450-02) and 10 ng/ml NT-3 (Peprotech; #AF450-03). During the differentiation process, cells were split once on Poly-L-Lysin/ Laminin-coated plates when reaching 100% confluency. For each experiment 4 6-well plates were first coated in 1 µg/ml Poly-L-Lysin (Sigma-Aldrich; #P5899) for 30 min at 37°C. Subsequently, plates were washed 3x with PBS before being coated with 2 µg/ml Laminin (Sigma-Aldrich; #11243217001) for at least 8 h at RT in the dark. Before cells were seeded, plates were washed twice in PBS. Cell splitting was performed as described above. Differentiations were regularly monitored for differentiation progress using an inverted light microscope (Carl Zeiss; #4001648). A graphical overview of the differentiation process is presented in Extended data figure 1. Characterization of the emerging iPSC-derived neurons was performed by immunofluorescent stainings for ß-III-tubulin, Neurofilament and CRLF3 as described above (table 3).

Establishment of survival assay

Different concentrations of rotenone as a pro-apoptotic stressor and EV-3 as an anti-apoptotic protectant were tested. For final experiments rotenone (Sigma-Aldrich; #R8875; dissolved in DMSO at stock concentration of 1,3 M) concentrations of 800 nM (for iPSC#1) and 1 µM (for iPSC#2) were applied for 18 h after treating cells with either 41,5 ng/ml (iPSC#1) or 33,3 ng/ml (iPSC#2) EV-3 (IBA GmbH, Göttingen, Germany) for 12 h. For each experiment one well of differentiations were treated with 0,006% DMSO as rotenone solvent control. After treatment periods, iPSC-derived neurons were prepared for FACS analysis as stated below.

FACS sample preparation and analysis

To collect samples for FACS analysis cell cultures were incubated in 0,25% Trypsin/EDTA for 3 min at 37°C before stopping the reaction with DMEM/FBS. Cells were scraped and resuspended by gentle pipetting before being transferred to falcon tubes. 2 ml DMEM/FBS were added and samples were centrifuged at 800 x g for 5 min. Samples were subsequently washed twice in PBS, with centrifugation steps between washing steps. In order to have samples for all treatment groups and to set FACS gates, only a subset of the cells were stained for further analysis. Table 4 shows the different treatment conditions and staining procedures employed for this protocol. Samples designated for live/dead

analysis were stained in Phantom dye Red 780 (Proteintech; #PD00002) for 30 min at 4°C according to the antibody list in table 3. Samples were subsequently diluted with 2 ml PBS + 0,1 % FBS and centrifuged at 800 x g for 5 min. Samples were washed one more time in PBS/FBS before being blocked alongside with unstained samples for at least 1 h at 4°C in PBS/0,5% BSA. 2 ml PBS were added and samples were centrifuged before a second PBS washing step. Subsequently, samples stained for ß-III-tubulin as neuronal marker were incubated with antibody according to table 3 overnight at 4°C. Samples that did not receive staining solution remained in blocking buffer. The next day 2 ml PBS were added to all falcons and the samples were centrifuged. After a second PBS washing step, cells were resuspended in FACS buffer (Containing PBS + 0,5% BSA + 2 mM EDTA) and strained through a 40 µm cell strainer (Sarstedt; #833945040) into FACS tubes (Fisher Scientific; #10579511). Samples were kept on ice until analysis with Sony cell sorter SH800S.

Table 4: FACS samples prepared for survival assays

Treatment	FACS sample
Control	Neg. control Phantom dye ß-III-tubulin ß-III/Phantom dye
Rotenone	Phantom dye ß-III/Phantom dye
EV-3 + rotenone	 ß-III/Phantom dye

FACS gates were set according to the forward and sideward scatter measured in the main gate for single-cell analysis. Gates for the selection of ß-III-tubulin-positive cells were set according to the unstained control samples. Phantom dye gates for live and dead cells were set according to the unstressed population. For all samples 100.000 cells were measured. Only ß-III-tubulin positive cells (i.e., neuron-like cells) were analysed for their survival according to Phantom dye staining.

FACS data is presented as boxplots showing the median cell survival, upper and lower quartile and whiskers representing 1,5 x interquartile ranges. Single data points are shown as circles within the boxplot. Cell survival data was normalized to the corresponding untreated control, which was set to 1.

Gene expression studies

RNA isolation and cDNA synthesis

For each treatment group in the survival assays cells from two wells of a 6-well plate were pelleted for further molecular analysis. RNA was isolated by means of Trizole/Chloroform protocol as described

previously (Knorr *et al.*, 2020). In brief, 1 ml Trizole (Thermo Fisher Scientific; #15596026) was added to each cell pellet and cells were disrupted in a tissue lyser. 200 µl Chloroform (Labsolute; #2475) was added and the samples were shaken vigorously for 20 sec in tissue lyser. Samples were incubated on ice for 15 min before centrifugation at 12.000 x g for 15 min at 4°C. The top translucent phase of each sample was transferred to a fresh Eppendorf cup and mixed with 1 ml ice-cold 75% EtOH. Samples were incubated at -20°C for at least 1 h before centrifugation at 10.000 x g for 15 min at 4°C. The resulting RNA pellet was washed three times in ice-cold EtOH before pellets were dried and resuspended in 30 µl ddH2O. RNA concentrations were measured by Nanodrop (Thermo Fisher Scientific).

cDNA was synthesised using the LunaScript RT SuperMixKit (New England BioLabs; #E3010) according to the manufactures instructions. For all samples 1 µg RNA was reverse transcribed.

qPCR

qPCR analyses of transcripts from *BAX, Caspase 3, BCL-2* and *CRLF3* were run using specific primers (see oligonucleotide list Table 1). The housekeeping gene (HKG) *b-Actin* was used as reference. All primers were analysed for their efficiencies previously. All samples were loaded in triplicates and (-) RT controls and water were run as negative controls on each plate. qPCRs reactions were prepared with final concentrations of 5 µl Luna® Universal qRT-PCR Master Mix (New England Bio- Lab; #M3003), 0,1 mM forward and reverse primers and 10 ng cDNA. qPCRs were pipetted in a 96-well clear well plates (StarLab; #E1403-5200) and run using a Bio-Rad CFX Connect Real-Time system (Bio-Rad; #1855201). The following qPCR program was employed for specific gene amplification (see table 5).

Table 5: qPCR program used for this study

	Step	Temperature [°C]	Time [s]	
	Initial denaturation	95	180	
PCR reaction	Denaturation	95	10	x40
	Annealing	61	30	
	Elongation	72	30	
Melting curve	Denaturation	95	60	
	Annealing	55	60	
	Melting curve	55	10	0.5 °C per cycle up to 95 °C

Ct values were analysed using the Pfaffl method [59] and data was normalized to the corresponding HKG value of each sample and further to the corresponding gene of interest (GOI) control value. Relative gene expression data is represented as Bar plots showing the geometric mean and standard deviations.

CRLF3 immunostaining of iPSC-derived neurons

iPSC-derived neurons were grown on glass coverslips and fixed on day 30 of differentiation. Cell staining was performed as described above using primary antibodies for Neurofilament 200 and CRLF3 (See antibody list table 3) and Dapi (1:1000 in H_2O; Sigma Aldrich; #D9564) as nuclear marker. Images were taken using Leica SP8 confocal microscope (Leica Microsystems). Images were further processed using ImageJ.

Quantification and statistical analysis

Statistical analyses of all experiments conducted in this study was performed using R Studio [60, 61] and pairwise permutation test (two-tailed) within the packages coin and rcompanion [62, 63]. In order to avoid false-positive results due to multiple comparisons, Benjamini Hochberg correction was included in all statistical calculations. Significant differences are shown by differing letters (e.g. a is significantly different to b but not to ab). All data presented was collected from independent experiments. Only experiments with a minimum of 5 % survival loss in rotenone treated cultures were included into final analysis. Exact n values (defined as number of individually measured experiments) for each experiment can be found in the figure legends.

Results

Characterization of CRISPR-generated cell lines

In order to generate CRLF3 deficient cell lines, two independent human iPSC lines (#1 and #2, female and male respectively) were transfected with a plasmid coding for the piggyBac transposase, and a piggyBac vector containing Cas9-GFP and gRNAs to target exon 3 of the gene (see Fig 1A). Fig 1 shows a representation of the mutation characterizations performed. Only cell lines showing two types of mutation (corresponding to alleles A and B) were considered for further analysis. Both generated KO lines contained frameshift-inducing mutations at the scaffold site resulting in termination of protein translation due to premature stop codons. Expression of CRLF3 protein in the generated cell lines was analysed by Western blots. Both clonal KO lines generated from iPSC#1 and iPSC#2 entirely lack CRLF3 protein (Fig 1 C). In contrast, CRLF3-related immunoreactivity of the expected size of 55 kDa was detected as single bands of WT and Ig-Ctrl cells. αTubulin was probed as loading control and detected at the expected size in all cell lines. The newly generated clonal lines all express GFP homogeneously, allowing to monitor cross-contaminations with other cell lines (see Fig 1 D). Both Ig-Ctrl and KO cells from iPSC#1 and #2 were characterized for their pluripotent state (see Supp Fig. 1). All four lines retained the capacity for spontaneous differentiation into all three germ layers (Supp Fig 1 A) and exhibited staining for core pluripotency markers (Supp Fig 1 B).

EV-3 induces CRLF3-mediated protection of human iPSC-derived neurons

EpoR, but not ßcR, is expressed in iPSC-derived neurons used in this study (data not shown). Instead of Epo, which activates both classical EpoR and alternative tissue-protective receptors, we used the human natural Epo splice variant EV-3. EV-3 is unable to activate classical EpoR, stimulates anti-apoptotic mechanisms in mammalian neurons (via alternative Epo receptors) and has been demonstrated to mediate protection of insect neurons via binding to CRLF3 [10, 48, 64]. Before starting with main experiments, we established protocols for apoptosis induction with rotenone and EV-3-mediated cell protection by testing different concentrations and exposure periods separately for both lines (Supp Fig 2 shows results of these experiments). Best combinations for apoptosis induction and neuroprotection differed between the two lines and led to the following protocols for subsequent survival assays: iPSC#1-derived neurons were exposed to 41,5 ng/ml EV-3 starting 12 h before exposure to 800 nM rotenone for 18 h. iPSC#2-derived neurons were exposed to 33,3 ng/ml EV-3 starting 12 h before exposure to 1µM rotenone. In these preliminary experiments EV-3 protected neurons from both iPSC lines during rotenone-induced chemical hypoxia indicating that alternative Epo receptors activate the protective intracellular pathways.

For core experiments WT, Ig-Ctrl and CRLF3 KO cells from both lines were differentiated for 30 days and subsequently treated with EV-3 according to our previous findings (41,5 ng/ml iPSC#1 / 33,3 ng/ml iPSC#2) EV-3. After 12 h 800 nM (iPSC#1) or 1 µM (iPSC#2) rotenone was added for 18 h before samples were collected for FACS analysis. 100.000 cells per sample were measured in five repetitions for each cell line. Of these, only ß-III-tubulin immunopositive cells were included in the quantitative analysis to circumvent variations resulting from divergent differentiation efficiencies (differentiation efficiencies are displayed in Supp. Fig 3). Neuron-specific ß-III-tubulin staining of iPSC-derived neurons at day 30 of differentiation labelled extensive axonal networks of all lines (Fig 2).

Exposure to 800 nM rotenone reduced survival of WT, Ig-Ctrl and *CRLF3*-mutated iPSC#1-derived neurons (Fig 3 D, E, F). WT neurons were particularly sensitive to rotenone treatment (median relative survival 0,68) compared to Ig-Ctrl (0,88) and KO (0,87) neurons. The deleterious effect of rotenone was completely prevented by EV-3 (41,5 ng/ml) in WT and Ig-Ctrl neurons (median relative survival 0.96 and 0,99). In contrast, EV-3 had no protective effect on *CRLF3* KO neurons (median relative survival 0,83) since cell survival was not different from rotenone-treated cultures (median relative survival 0,87).

Given that rotenone solutions are prepared in DMSO, control experiments with 0,006 % DMSO (represents the final concentration during treatments with 1 µM rotenone) had no impact on the survival of WT and Ig-Ctrl neurons compared to untreated cultures (median relative survival 0,99 and 1,02). Survival of *CRLF3* KO was slightly, yet significantly, decreased (median relative survival 0,96). However, the toxic effect of DMSO in these cells was not as severe as in rotenone exposed cultures (median relative survival 0,87).

iPSC-derived neurons originating from iPSC#2 show similar results in survival assays as cells originating from iPSC#1 (Figure 3 G, H, I). Exposure to 1 µM rotenone, significantly decreased survival of WT, Ig-Ctrl and *CRLF3* KO neurons in comparison to untreated control cells (median survival 0,90, 0,92, 0,74 respectively). Treatment of WT and Ig-Ctrl cells with 33,3 ng/ml EV-3 rescued iPSC-derived neurons from rotenone-induced apoptosis, with cell survival of Ig-Ctrl cells being significantly increased to or beyond survival of untreated control cells (median survival 0,97 for WT and 1,04 for Ig-Ctrl cells). Treatment of *CRLF3* KO cells with EV-3 did not increase cell survival in comparison to sole rotenone exposure (0,78 median cell survival). Neurons derived from iPSC#2 reacted more strongly to DMSO treatment than iPSC#1 cells (see Supp. Fig. 4).

CRLF3 protein levels in apoptogenic and rescue conditions

Potential treatment-related alterations of CRLF3 protein levels in WT and Ig-Ctrl iPSC-derived neurons were analysed by Western blots. Samples from control and pharmacologically treated cultures of the same experiment were simultaneously analysed on the same gel and blot. Both antibodies labelled single bands at the expected molecular size (~55 kDa for both proteins) in each sample.

Exposure to rotenone increased CRLF3 levels in iPSC#1 WT (2,1 ± 0,7 fold) and Ig-Ctrl neurons (1,6 ± 0,2 fold) compared to untreated controls (Fig. 4 A,B). Rotenone-induced accumulation of CRLF3 was reduced by co-treatment with EV-3 in WT (1,5 ± 0,1 STDV, not significant compared to rotenone-only treatment) and Ig-Ctrl neurons (1,2 ± 0,1 STDV, significantly different from rotenone-only exposure). In contrast, CRLF3 levels were not affected by rotenone ± EV-3 exposure of WT and Ig-Ctrl neuron-like cells originating from iPSC#2 (Fig 4 C,D). In order to determine the localization of CRLF3 iPSC#1 -derived neurons, we labelled differentiated WT, Ig-Ctrl and *CRLF3* KO cells with Dapi and antibodies against neurofilament 200 and CRLF3. As shown in Fig. 4 E, all cell lines expressed neurofilament 200, which is generated in the cell body cytosol and transported into axons. CRLF3-immunoreactivity appeared in dot-like patterns in cell bodies and along axons of WT and Ig-Ctrl cells but not in *CRLF3* KO cells.

Effects of rotenone and rotenone/EV-3 –exposure on gene expression

We analysed the expression of pro- and anti-apoptotic genes in untreated, rotenone-exposed and rotenone plus EV-3-treated iPSC-derived neurons. Analysis included early pro-apoptotic *BAX*, late pro-apoptotic *Caspase 3*, anti-apoptotic *BCL-2* and *CRLF3*. Figure 5 displays the data as average relative gene expression with standard deviation. Given the comparatively low differentiation efficiency of iPSC#2,

these experiments were only performed with iPSC#1-derived cells, to assure a sufficiently high proportion of neuron-like cells in analysed samples.

Expression of each gene of interest is separately displayed in Fig. 5 A. Expression of pro-apoptotic *BAX* significantly increased during exposure to the apoptogenic rotenone stimulus in WT (1,7 fold ± 0,06 STDV) and Ig-Ctrl neurons (1,76 fold ± 0,46 STDV) compared to respective untreated cultures. Co-application of EV-3 prevented rotenone-induced *BAX* overexpression and caused a significant decrease of relative expression compared to untreated controls (WT 0,74 ± 0,06, Ig-Ctrl 0,74 ± 0,12 STDV). In contrast, *BAX* expression in CRLF3-deficient KO neurons was neither altered by rotenone (0,93 ± 0,56 STDV) nor by combined treatment with rotenone and EV-3 (1,16 ± 0,13 STDV). Expression of executioner caspase *Caspase 3* in WT cells significantly increased during rotenone exposure (1,47 ± 0,17 STDV) and was reduced below control level following exposure of rotenone with EV-3 (0,66 ± 0,11 STDV). Neither of the treatments altered *Caspase 3* expression in Ig-Ctrl cells. *CRLF3*-KO cells significantly increased *Caspase 3* expression during rotenone exposure (1,52 ± 0,74 STDV), with overexpression not being prevented by co-treatment with EV-3 (1,97 ± 0,75 STDV). *BCL-2* and *CRLF3* expression were not significantly altered by exposure to rotenone or rotenone plus EV-3 in WT, Ig-Ctrl and CRLF3 KO iPSC-derived neurons. However, *BCL-2* expression in rotenone/EV-3-treated WT (1,52 ± 0,18 STDV) and Ig-Ctrl cells (1,3 ± 0,32 STDV) seemed to be elevated, especially compared to rotenone-only treated cultures. WT and Ig-Ctrl lines also demonstrate slightly elevated CRLF3 expression (not significant) upon exposure to the rotenone stressor (1,46 ± 0,27 and 1,39 ± 0,27 STDV respectively).

For direct comparison of treatment-related changes in gene expressions, we rearranged the data in Figure 5 B and plotted it as the log2 of relative gene expression compared to untreated controls. While WT cells significantly increase the expression of both early and late apoptosis genes when stressed (0,55 ± 0,22 *Caspase 3* to 0,77 ± 0,07 *BAX*), Ig-Ctrl and KO cells overexpress either *BAX* or *Caspase 3* respectively. *BCL-2* expression was downregulated for all lines. When cells are treated with EV-3, the overexpression of pro-apoptotic genes is prevented and anti-apoptotic *BCL-2* is significantly overexpressed in WT and Ig-Ctrl cells (0,6 ± 0,4 and 0,38 ± 0,4 STDV respectively). *CRLF3*-KO cells overexpress *Caspase 3* when treated with EV-3 (1,29 ± 0,25 STDV). *BCL-2* and *BAX* expression remain elevated in comparison to control (0,31 ± 0,74 and 0,22 ± 0,18 STDV respectively).

Discussion

The cytokine Epo mediates neuroprotection and promotes regeneration in mammalian nervous systems. Animal models and clinical observations identified Epo as a promising treatment to prevent neurodegenerative cell loss. While Epo itself co-activates adverse effects such as overproduction of blood cells increasing the risk of thrombosis and promotion of tumour growth, some Epo-mimetics including EV-3 selectively stimulate tissue protection without activating homodimeric EpoR-associated side effects. Hence, identification and selective targeting of tissue-protective Epo receptors should be attempted for

therapies against neurodegenerative diseases. The present study identifies EV-3/CRLF3-signalling in human neurons as a promising neuroprotective option.

Previous studies on insects suggested that the evolutionary conserved orphan cytokine receptor CRLF3 may serve as neuroprotective receptor for Epo in the mammalian nervous system [6, 10]. CRLF3 has been associated with a variety of diseases including neurofibromatosis type I, cutaneous Leishmaniasis, cutaneous squamous cell carcinoma, amyotrophic lateral sclerosis, autism and cancer [11, 14, 16, 65, 66]. Apart from this, studies on PC12 cells and iPSC-derived cerebral organoids indicated that CRLF3 regulates the development and differentiation of neurons [11]. However, concrete functions of CRLF3 remained unknown until its regulatory role in vertebrate hematopoiesis and particularly in mammalian thrombopoiesis were recently reported [8, 9], though without discovering the identity of its ligand. Insect CRLF3 initiates anti-apoptotic neuroprotective mechanisms upon activation with both human Epo and EV-3 [6, 10]. While the endogenous ligand for insect CRLF3 is still unknown [67] current knowledge suggests that CRLF3 is the only Epo/EV-3-responsive receptor in insects. In contrast, mammals express classical homodimeric EpoR activated by Epo and alternative tissue-protective Epo receptors activated by Epo and selective ligands such as EV-3. EV-3 is a natural splice variant that lacks the entire third exon of the *Epo* transcript which prevents activation of homodimeric EpoR and heteromeric EpoR/βcR [48, 68]. EV-3 is present in human serum and brain and elicits anti-apoptotic effects on rat hippocampal neurons [48]. Using EV-3 in our study prevented the activation of EpoR which is expressed in both iPSC lines and iPSC-derived neurons used in this study, while ßcR expression was only detected in undifferentiated iPSC. Demonstrating that EV-3 mediates neuroprotection via human CRLF3 not only deorphanizes CRLF3 but also identifies the previously proposed neuroprotective receptor for EV-3. Since Epo can be regarded as the more general ligand that stimulates both erythropoiesis and tissue protection and insect CRLF3 is activated by both Epo and EV-3, it can be assumed that human CRLF3 will also be stimulated by EV-3 and Epo.

EV-3 protects insect and rat neurons at similar or lower concentrations than Epo [10, 48, 50, 51, 64]**.** Both Epo and EV-3 protect neurons in an optimum-type dose response, with both lower and higher concentrations being less neuroprotective and very high concentrations even exerting deleterious effects on cell survival [10, 48, 64, 69–71]. Optimal concentrations may vary between species (e.g. brain neurons of *L. migratoria* and *T. castaneum*) and even between different cell types within the same organism and tissue (brain neurons and glia of *L. migratoria*). Such differences were also detected between the two lines of iPSC-derived neurons used in our study. While rotenone-stressed neurons of iPSC#1 were best protected by 41,5 ng/ml EV-3, the most neuroprotective concentration for iPSC#2 was 33,3 ng/ml. Apoptosis-induction with rotenone has frequently been used in studies with various cell types including neurons and Epo-mediated neuroprotection of rotenone-stressed neurons has been reported in vitro [72, 73]. It is important to note, that iPSC#2 cells differentiated not as efficiently as cells originating from iPSC#1. This could account for the higher concentration of rotenone required, in order to sufficiently stress the cells for a significant portion of apoptosis induction.

To our knowledge, the neuroprotective role of Epo or EV-3 in human neurons has not been directly studied. Aiming to explore the potential of Epo mediated cytoprotection in human cells, we generated iPSC-derived neurons that recapitulate essential aspects of in vivo human neurons. Both lines of iPSC-derived neurons assumed neuron-like morphologies and expressed neuron-specific proteins including β–III-tubulin and neurofilament 200. We strived to understand if (1) EV-3 elicits neuroprotective functions in human neuron-like cells and (2) if this neuroprotection requires the presence of human CRLF3. We demonstrate that EV-3 administration 12 h before and during rotenone-exposure protects WT and Ig-Ctrl neuron-like cells from stress-induced apoptosis. For both cell lines used in this study the apoptotic effect of rotenone was entirely compensated, resulting in cell survival close to control (untreated cells) levels. Importantly, EV-3 mediated neuroprotection was completely absent in CRLF3 KO cells. This data provides evidence that EV-3 (and likely also Epo) and CRLF3 represent a ligand-receptor pair that stimulates protective mechanisms in human cells.

Physiological and/or pathological stress elevates *EpoR* expression in neuronal cell cultures [74–76], in spinal cord [77] and brain [74, 78, 79]. Additionally, increased presence of EpoR/βcR in renal cells after ischemic reperfusion injury were also reported [80]. Cell-protective Epo receptors were either upregulated [81] or downregulated [80] by the presence of Epo or receptor-activating Epo mimetic molecules in some studies. Hence, we asked whether *CRLF3* expression in iPSC-derived neurons was similarly affected by rotenone-induced stress and EV-3 application. Western blot analysis of iPSC#1 WT and Ig-Ctrl neurons indicated increased CRLF3 levels following rotenone-exposure and partial prevention of this increase by co-application of EV-3. In contrast to the survival assays that selectively analysed neuron-like cells, Western blot analysis non-selectively included all cells in these cultures. Nevertheless, the data suggest that CRLF3 is upregulated under apoptogenic conditions. The presence of EV-3 reduced apoptosis induction by rotenone causing no or reduced upregulation of CRLF3 protein. However, no rotenone and/or EV-3 effects on CRLF3 levels were detected in iPSC#2 WT and Ig-Ctrl neurons. This result is probably caused by lower differentiation efficiency of iPSC#2 (compared to iPSC#1) and more diluted effects by higher portions of non-neuronal cell types.

For a basic characterization of EV-3/CRLF3-mediated anti-apoptotic mechanisms at play we analysed the expression of pro- and anti-apoptotic proteins in neuron-like cells derived from iPSC#1. Initiation and progress of apoptosis has been correlated with differential gene expression of *Caspase 3* and *BAX* [82–85]. Our data suggest that 18 h rotenone-induced stress leads to overexpression of both “early” and “late” pro-apoptotic genes (namely *BAX* and *Caspase 3*, respectively) in WT cells. It is intriguing that in contrast to iPSC#1 WT cells, iPSC#1 Ig-Ctrl neuron-like cells seem to initiate apoptosis later, which is underlined by the lack of *Caspase 3* overexpression but a pronounced overexpression of the early apoptosis marker *BAX*. For both WT and Ig-Ctrl cells, EV-3 prevented rotenone-induced elevation of *Caspase 3* and/or *BAX.* Additionally, anti-apoptotic *BCL-2* expression increased in cells treated with EV-3. This data suggests that EV-3 mediates neuroprotection by upregulation of anti- and downregulation of pro-apoptotic genes, enabling the cells to counteract apoptotic processes induced by rotenone. Interestingly, the iPSC#1 KO cells analysed in this study do not display these protective gene expression profiles. *CRLF3*-KO cells show a rather dysregulated transcriptional program, indicated by a high variance amongst the different

samples. Rotenone treatment did not result in overexpression of *BAX* but in a clear overexpression of *Caspase 3*. Neither *BAX* nor anti-apoptotic *BCL-2* were differentially expressed when KO cells are treated with EV-3 and *Caspase 3* remained strongly overexpressed. The lack of *BCL-2* overexpression in EV-3 treated cells together with the high variances observed in gene expression profiles not only underline the absence of any EV-3 mediated cell-protective effects but also points towards regulatory functions of CRLF3 in cell homeostasis.

The data presented here identify human CRLF3 as a receptor for the natural Epo splice variant EV-3. Expression of CRLF3 in various human tissues suggests that CRLF3-stimulated transduction pathways can interfere with apoptotic processes in other cell types besides neurons. With respect to the cytokine-mediated regulation of hematopoiesis, Epo likely promotes both erythrocyte and thrombocyte production via EpoR and CRLF3, whereas EV-3/CRLF3 signalling is selective for thrombopoiesis, providing the opportunity to differentially regulate the production of different hemocytes.

The involvement of CRLF3 in human iPSC-derived neuroprotection will initiate a variety of studies to uncover the protective molecular pathways. Epo-mediated protection of mammalian neurons reported in numerous previous studies may have been mediated by EpoR and/or EpoR/βcR and/or CRLF3 unless control experiments associated the observed neuroprotective effects with the activation of a particular type of Epo-responsive receptor. Implication of CRLF3 in anti-apoptotic and cell-protective mechanisms will facilitate the identification of additional Epo-like ligands to be applied as specific neuro- or other tissue-protective agents. Using iPSC-derived cell types from healthy and diseased donors enables focussed studies on cell-protective mechanisms in cell-specific molecular settings.

References

1. Dame C, Wolber EM, Freitag P, Hofmann D, Bartmann P, Fandrey J (2003) Thrombopoietin gene expression in the developing human central nervous system. Dev Brain Res 143:217–223. https://doi.org/10.1016/S0165-3806(03)00134-2
2. Schäbitz WR, Kollmar R, Schwaninger M, Juettler E, Bardutzky J, Schölzke MN, Sommer C, Schwab S (2003) Neuroprotective effect of granulocyte colony-stimulating factor after focal cerebral ischemia. Stroke 34:745–751. https://doi.org/10.1161/01.STR.0000057814.70180.17
3. Schneider A, Krüger C, Steigleder T, Weber D, Pitzer C, Laage R, Aronowski J, Maurer MH, Gassler N, Mier W, Hasselblatt M, Kollmar R, Schwab S, Sommer C, Bach A, Kuhn HG, Schäbitz WR (2005) The hematopoietic factor G-CSF is a neuronal ligand that counteracts programmed cell death and drives neurogenesis. J Clin Invest 115:2083–2098. https://doi.org/10.1172/JCI23559
4. Byts N, Samoylenko A, Woldt H, Ehrenreich H, Sirén AL (2006) Cell type specific signalling by hematopoietic growth factors in neural cells. Neurochem Res 31:1219–1230. https://doi.org/10.1007/s11064-006-9149-0
5. Boulay JL, O'Shea JJ, Paul WE (2003) Molecular phylogeny within type I cytokines and their cognate receptors. Immunity 19:159–163

6. Hahn N, Büschgens L, Schwedhelm-Domeyer N, Bank S, Geurten BRH, Neugebauer P, Massih B, Göpfert MC, Heinrich R (2019) The Orphan Cytokine Receptor CRLF3 Emerged With the Origin of the Nervous System and Is a Neuroprotective Erythropoietin Receptor in Locusts. Front Mol Neurosci 12:. https://doi.org/10.3389/fnmol.2019.00251
7. Liongue C, Ward AC (2007) Evolution of Class I cytokine receptors. BMC Evol Biol 7:. https://doi.org/10.1186/1471-2148-7-120
8. Taznin T, Perera K, Gibert Y, Ward AC, Liongue C (2022) Cytokine Receptor-Like Factor 3 (CRLF3) Contributes to Early Zebrafish Hematopoiesis. Front Immunol 13:1–11. https://doi.org/10.3389/fimmu.2022.910428
9. Bennett C, Lawrence M, Guerrero JA, Stritt S, Waller AK, Yan Y, Mifsud RW, Ballester-Beltran J, Baig AA, Mueller A, Mayer L, Warland J, Penkett CJ, Akbari P, Moreau T, Evans AL, Mookerjee S, Hoffman GJ, Saeb-Parsy K, Adams D, Couzens AL, Bender M, Erber W, Nieswandt B, Read RJ, Ghevaert C (2022) CRLF3 plays a key role in the final stage of platelet genesis and is a potential therapeutic target for thrombocythaemia. Blood. https://doi.org/10.1182/blood.2021013113
10. Hahn N, Knorr DY, Liebig J, Wüstefeld L, Peters K, Büscher M, Bucher G, Ehrenreich H, Heinrich R (2017) The Insect Ortholog of the Human Orphan Cytokine Receptor CRLF3 Is a Neuroprotective Erythropoietin Receptor. Front Mol Neurosci 10:1–11. https://doi.org/10.3389/fnmol.2017.00223
11. Wegscheid ML, Anastasaki C, Hartigan KA, Cobb OM, Papke JB, Traber JN, Morris SM, Gutmann DH (2021) Patient-derived iPSC-cerebral organoid modeling of the 17q11.2 microdeletion syndrome establishes CRLF3 as a critical regulator of neurogenesis. Cell Rep 36:109315. https://doi.org/10.1016/j.celrep.2021.109315
12. Hashimoto Y, Muramatsu K, Kunii M, Yoshimura S, Yamada M, Sato T, Ishida Y, Harada R, Harada A (2012) Uncovering genes required for neuronal morphology by morphology-based gene trap screening with a revertible retrovirus vector. FASEB J 26:4662–4674. https://doi.org/10.1096/fj.12-207530
13. Yang F, Xu Y-P, Li J, Duan S-S, Fu Y-J, Zhang Y, Zhao Y, Qiao W-T, Chen Q-M, Geng Y-Q, Che C-Y, Cao Y-L, Wang Y, Zhang L, Long L, He J, Cui Q-C, Chen S-C, Wang S-H, Liu L (2009) Cloning and characterization of a novel intracellular protein p48.2 that negatively regulates cell cycle progression. Int J Biochem Cell Biol 41:2240–2250. https://doi.org/10.1016/j.biocel.2009.04.022
14. Dang C, Gottschling M, Manning K, O'Currain E, Schneider S, Sterry W, Stockfleth E, Nindl I (2006) Identification of dysregulated genes in cutaneous squamous cell carcinoma. Oncol Rep 16:513–519. https://doi.org/10.3892/or.16.3.513
15. Cirulli ET, Lasseigne BN, Petrovski S, Sapp PC, Dion PA, Leblond CS, Couthouis J, Lu YF, Wang Q, Krueger BJ, Ren Z, Keebler J, Han Y, Levy SE, Boone BE, Wimbish JR, Waite LL, Jones AL, Carulli JP, Day-Williams AG, Staropoli JF, Xin WW, Chesi A, Raphael AR, McKenna-Yasek D, Cady J, De Jong JMBV, Kenna KP, Smith BN, Topp S, Miller J, Gkazi A, Al-Chalabi A, van den Berg LH, Veldink J, Silani V, Ticozzi N, Shaw PJ, Baloh RH, Appel S, Simpson E, Lagier-Tourenne C, Pulst SM, Gibson S, Trojanowski JQ, Elman L, McCluskey L, Grossman M, Shneider NA, Chung WK, Ravits JM, Glass JD,

Sims KB, Van Deerlin VM, Maniatis T, Hayes SD, Ordureau A, Swarup S, Landers J, Baas F, Allen AS, Bedlack RS, Harper JW, Gitler AD, Rouleau GA, Brown R, Harms MB, Cooper GM, Harris T, Myers RM, Goldstein DB, Hardiman O, McLaughlin RL, Mazzini L, Blair IP, Williams KL, Nicholson GA, Al-Sarraj S, King A, Scotter EL, Troakes C, Vance C, D'Alfonso S, Duga S, Corrado L, ten Asbroek AL, Calini D, Colombrita C, Ratti A, Tiloca C, Wu Z, Asress S, Polak M, Diekstra F, van Rheenen W, Danielson EW, Fallini C, Keagle P, Lewis EA, Kost J, Sorarù G, Bertolin C, Querin G, Castellotti B, Gellera C, Pensato V, Taroni F, Cereda C, Gagliardi S, Ceroni M, Lauria G, de Belleroche J, Comi GP, Corti S, Del Bo R, Turner MR, Talbot K, Pall H, Morrison KE, Esteban-Pérez J, García-Redondo A, Muñoz-Blanco JL (2015) Exome sequencing in amyotrophic lateral sclerosis identifies risk genes and pathways. Science (80-) 347:1436–1441. https://doi.org/10.1126/science.aaa3650

16. Castellucci LC, Almeida L, Cherlin S, Fakiola M, Francis RW, Carvalho EM, Santos da Hora A, do Lago TS, Figueiredo AB, Cavalcanti CM, Alves NS, Morais KLP, Teixeira-Carvalho A, Dutra WO, Gollob KJ, Cordell HJ, Blackwell JM (2021) A Genome-wide Association Study Identifies SERPINB10, CRLF3, STX7, LAMP3, IFNG-AS1, and KRT80 As Risk Loci Contributing to Cutaneous Leishmaniasis in Brazil. Clin Infect Dis 72:e515–e525. https://doi.org/10.1093/cid/ciaa1230
17. Jelkmann W, Metzen E (1996) Erythropoietin in the control of red cell production. Ann Anat 178:391–403. https://doi.org/10.1016/S0940-9602(96)80124-5
18. Constantinescu SN, Ghaffari S, Lodish HF (1999) The erythropoietin receptor: Structure, activation and intracellular signal transduction. Trends Endocrinol. Metab. 10:18–23
19. Lundby C, Olsen NV (2011) Effects of recombinant human erythropoietin in normal humans. J. Physiol. 589:1265–1271
20. Chateauvieux S, Grigorakaki C, Morceau F, Dicato M, Diederich M (2011) Erythropoietin, erythropoiesis and beyond. Biochem Pharmacol 82:1291–1303. https://doi.org/10.1016/j.bcp.2011.06.045
21. Ghezzi P, Brines M (2004) Erythropoietin as an antiapoptotic, tissue-protective cytokine. Cell Death Differ. 11:S37–S44
22. Zhang Y, Wang L, Dey S, Alnaeeli M, Suresh S, Rogers H, Teng R, Noguchi CT (2014) Erythropoietin action in stress response, tissue maintenance and metabolism. Int. J. Mol. Sci. 15:10296–10333
23. Yu X, Shacka JJ, Eells JB, Suarez-quian C, Przygodzki RM, Lin C, Nikodem VM, Hempstead B, Flanders KC, Costantini F, Noguchi CT (2002) Erythropoietin receptor signalling is required for normal brain development. 516:505–516
24. Genc S, Koroglu TF, Genc K (2004) Erythropoietin and the nervous system. Brain Res 1000:19–31. https://doi.org/10.1016/j.brainres.2003.12.037
25. Kretz A, Happold CJ, Marticke JK, Isenmann S (2005) Erythropoietin promotes regeneration of adult CNS neurons via Jak2/Stat3 and PI3K/AKT pathway activation. Mol Cell Neurosci 29:569–579. https://doi.org/10.1016/j.mcn.2005.04.009
26. Morishita E, Narita H, Nishida M, Kawashima N, Yamagishi K, Masuda S, Nagao M, Hatta H, Sasaki R (1996) Anti-Erythropoietin Receptor Monoclonal Antibody: Epitope Mapping, Quantification of the

Soluble Receptor, and Detection of the Solubilized Transmembrane Receptor and the Receptor-Expressing Cells. Blood 88:465–471

27. Miskowiak K, Inkster B, O'Sullivan U, Selvaraj S, Goodwin GM, Harmer CJ (2008) Differential effects of erythropoietin on neural and cognitive measures of executive function 3 and 7 days post-administration. Exp Brain Res 184:313–321. https://doi.org/10.1007/s00221-007-1102-1
28. Miskowiak K, O'Sullivan U, Harmer CJ (2007) Erythropoietin enhances hippocampal response during memory retrieval in humans. J Neurosci 27:2788–2792. https://doi.org/10.1523/JNEUROSCI.5013-06.2007
29. Miskowiak KW, Carvalho AF, Vieta E, Kessing L V. (2016) Cognitive enhancement treatments for bipolar disorder: A systematic review and methodological recommendations. Eur. Neuropsychopharmacol. 26:1541–1561
30. Kästner A, Grube S, El-Kordi A, Stepniak B, Friedrichs H, Sargin D, Schwitulla J, Begemann M, Giegling I, Miskowiak KW, Sperling S, Hannke K, Ramin A, Heinrich R, Gefeller O, Nave KA, Rujescu D, Ehrenreich H (2012) Common variants of the genes encoding erythropoietin and its receptor modulate cognitive performance in schizophrenia. Mol Med 18:1029–1040. https://doi.org/10.2119/molmed.2012.00190
31. Chong ZZ, Shang YC, Mu Y, Cui S, Yao Q, Maiese K (2013) Targeting erythropoietin for chronic neurodegenerative diseases. Expert Opin Ther Targets 17:707–720. https://doi.org/10.1517/14728222.2013.780599
32. Maiese K, Chong ZZ, Shang YC (2008) RAVES AND RISKS FOR ERYTHROPOIETIN. Cytokine Growth Factor Rev 19:145–155
33. Rey F, Balsari A, Giallongo T, Ottolenghi S, Di Giulio AM, Samaja M, Carelli S (2019) Erythropoietin as a Neuroprotective Molecule: An Overview of Its Therapeutic Potential in Neurodegenerative Diseases. ASN Neuro 11
34. Ehrenreich H, Weissenborn K, Prange H, Schneider D, Weimar C, Wartenberg K, Schellinger PD, Bohn M, Becker H, Wegrzyn M, Jähnig P, Herrmann M, Knauth M, Bähr M, Heide W, Wagner A, Schwab S, Reichmann H, Schwendemann G, Dengler R, Kastrup A, Bartels C (2009) Recombinant human erythropoietin in the treatment of acute ischemic stroke. Stroke 40:. https://doi.org/10.1161/STROKEAHA.109.564872
35. Pedroso I, Bringas Vega ML, Aguiar A, Morales L, Álvarez M, Valdés PA, Álvarez L (2012) Use of Cuban recombinant human erythropoietin in Parkinson's disease treatment. MEDICC Rev 14:11–17. https://doi.org/10.37757/mr2012v14.n1.4
36. Cao Y (2013) Erythropoietin in cancer: A dilemma in risk therapy. Trends Endocrinol. Metab. 24:190–199
37. Hardee ME, Arcasoy MO, Blackwell KL, Kirkpatrick JP, Dewhirst MW (2006) Erythropoietin biology in cancer. Clin. Cancer Res. 12:332–339
38. Leist M, Ghezzi P, Grasso G, Bianchi R, Villa P, Fratelli M, Savino C, Bianchi M, Nielsen J, Gerwien J, Kallunki P, Larsen AK, Helboe L, Christensen S, Pedersen LO, Sfacteria A, Erbayraktar S (2004)

Derivatives of Erythropoietin That Are Tissue Protective But Not Erythropoietic. 305:239–243

39. Brines M, Patel NSA, Villa P, Brines C, Mennini T, De Paola M, Erbayraktar Z, Erbayraktar S, Sepodes B, Thiemermann C, Ghezzi P, Yamin M, Hand CC, Xie QW, Coleman T, Cerami A (2008) Nonerythropoietic, tissue-protective peptides derived from the tertiary structure of erythropoietin. Proc Natl Acad Sci U S A 105:10925–10930. https://doi.org/10.1073/pnas.0805594105
40. Ueba H, Brines M, Yamin M, Umemoto T, Ako J, Momomura SI, Cerami A, Kawakami M (2010) Cardioprotection by a nonerythropoietic, tissue-protective peptide mimicking the 3D structure of erythropoietin. Proc Natl Acad Sci U S A 107:14357–14362. https://doi.org/10.1073/pnas.1003019107
41. Wu Y, Zhang J, Liu F, Yang C, Zhang Y, Liu A, Shi L, Wu Y, Zhu T, Nicholson ML, Fan Y, Yang B (2013) Protective effects of HBSP on ischemia reperfusion and cyclosporine a induced renal injury. Clin Dev Immunol 2013:. https://doi.org/10.1155/2013/758159
42. Brines M, Grasso G, Fiordaliso F, Sfacteria A, Ghezzi P, Fratelli M, Latini R, Xie Q, Smart J, Pobre E, Diaz D, Gomez D, Hand C, Coleman T, Cerami A (2004) Erythropoietin mediates tissue protection through an erythropoietin and common b -subunit heteroreceptor. PNAS 101:
43. Chamorro ME, Wenker SD, Vota DM, Vittori DC, Nesse AB (2013) Signaling pathways of cell proliferation are involved in the differential effect of erythropoietin and its carbamylated derivative. Biochim Biophys Acta - Mol Cell Res 1833:1960–1968. https://doi.org/10.1016/j.bbamcr.2013.04.006
44. Miller JL, Church TJ, Leonoudakis D, Lariosa-Willingham K, Frigon NL, Tettenborn CS, Spencer JR, Punnonen J (2015) Discovery and characterization of nonpeptidyl agonists of the tissue-protective erythropoietin receptors. Mol Pharmacol 88:357–367. https://doi.org/10.1124/mol.115.098400
45. Ding J, Wang J, Li QY, Yu JZ, Ma CG, Wang X, Lu CZ, Xiao BG (2017) Neuroprotection and CD131/GDNF/AKT Pathway of Carbamylated Erythropoietin in Hypoxic Neurons. Mol Neurobiol 54:5051–5060. https://doi.org/10.1007/s12035-016-0022-0
46. Nadam J, Navarro F, Sanchez P, Moulin C, Georges B, Laglaine A, Pequignot J, Morales A, Ryvlin P, Bezin L (2007) Neuroprotective effects of erythropoietin in the rat hippocampus after pilocarpine-induced status epilepticus. 25:412–426. https://doi.org/10.1016/j.nbd.2006.10.009
47. Sanchez PE, Navarro FP, Fares RP, Nadam J, Georges B, Moulin C, Le Cavorsin M, Bonnet C, Ryvlin P, Belmeguenai A, Bodennec J, Morales A, Bezin L (2009) Erythropoietin receptor expression is concordant with erythropoietin but not with common β chain expression in the rat brain throughout the life span. J Comp Neurol 514:403–414. https://doi.org/10.1002/cne.22020
48. Bonnas C, Wüstefeld L, Winkler D, Kronstein-wiedemann R, Dere E, Specht K, Boxberg M, Tonn T, Ehrenreich H (2017) EV-3, an endogenous human erythropoietin isoform with distinct functional relevance. Sci Rep 7:1–15. https://doi.org/10.1038/s41598-017-03167-0
49. Ostrowski D, Heinrich R (2018) Alternative Erythropoietin Receptors in the Nervous System. J Clin Med 7:. https://doi.org/10.3390/jcm7020024

50. Miljus N, Heibeck S, Jarrar M, Micke M, Ostrowski D, Ehrenreich H, Heinrich R (2014) Erythropoietin-mediated protection of insect brain neurons involves JAK and STAT but not PI3K transduction pathways. Neuroscience 258:218–227. https://doi.org/10.1016/j.neuroscience.2013.11.020
51. Miljus N, Massih B, Weis M, Rison V, Bonnas C, Sillaber I, Ehrenreich H, Geurten B, Heinrich R (2017) Neuroprotection and endocytosis: erythropoietin receptors in insect nervous systems. J Neurochem 141:63–74. https://doi.org/10.1111/jnc.13967
52. Rodriguez-Polo I, Stauske M, Becker A, Bartels I, Dressel R, Behr R (2019) Baboon induced pluripotent stem cell generation by piggyBac transposition of reprogramming factors. Primate Biol 6:75–86. https://doi.org/10.5194/pb-6-75-2019
53. Stauske M, Polo IR, Haas W, Knorr DY, Borchert T, Streckfuss-bömeke K, Dressel R, Bartels I, Tiburcy M, Zimmermann W, Behr R (2020) Non-Human Primate iPSC Generation, Cultivation, and Cardiac Differentiation under Chemically Defined Conditions. Cells 9:
54. Doss MX, Sachinidis A (2019) Current Challenges of iPSC-Based Disease Modeling and Therapeutic Implications. Cells 8:403. https://doi.org/10.3390/cells8050403
55. Wiegand C, Banerjee I (2019) Recent advances in the applications of iPSC technology. Curr. Opin. Biotechnol. 60:250–258
56. Rodriguez-Polo I, Mißbach S, Petkov S, Mattern F, Maierhofer A, Grządzielewska I, Tereshchenko Y, Urrutia-Cabrera D, Haaf T, Dressel R, Bartels I, Behr R (2021) A piggyBac-based platform for genome editing and clonal rhesus macaque iPSC line derivation. Sci Rep 11:15439. https://doi.org/10.1038/s41598-021-94419-7
57. Debowski K, Warthemann R, Lentes J, Salinas-Riester G, Dressel R, Langenstroth D, Gromoll J, Sasaki E, Behr R (2015) Non-viral generation of marmoset monkey iPS cells by a six-factor-in-one-vector approach. PLoS One 10:118424. https://doi.org/10.1371/journal.pone.0118424
58. Qi Y, Zhang X-J, Renier N, Wu Z, Atkin T, Sun Z, Ozair MZ, Tchieu J, Zimmer B, Fattahi F, Ganat Y, Azevedo R, Zeltner N, Brivanlou AH, Karayiorgou M, Gogos J, Tomishima M, Tessier-Lavigne M, Shi S-H, Studer L (2017) Combined small-molecule inhibition accelerates the derivation of functional, early-born, cortical neurons from human pluripotent stem cells. Nat Biotechnol 35:154. https://doi.org/10.1038/NBT.3777
59. Pfaffl MW (2001) A new mathematical model for relative quantification in real-time RT–PCR. Nucleic Acids Res 2001 29:2003–2007. https://doi.org/10.1111/j.1365-2966.2012.21196.x
60. Team Rs (2015) RStudio: Integrated Development for R. RStudio, Inc., Boston, MA
61. R Core Team (2019) An Introduction to dplR. Ind Commer Train 10:11–18. https://doi.org/10.1108/eb003648
62. Mangiafico SS (2019) Package ' rcompanion '
63. Zeileis A, Hornik K, Wiel MA, Hothorn T (2008) Implementing a class of permutation tests: The coin package. J Stat Softw 28:
64. Heinrich R, Günther V, Miljus N (2017) Erythropoietin-Mediated Neuroprotection in Insects Suggests a Prevertebrate Evolution of Erythropoietin-Like Signaling. In: Vitamins and Hormones. Academic Press

Inc., pp 181–196

65. Kehrer-Sawatzki H, Wahlländer U, Cooper DN, Mautner VF (2021) Atypical nf1 microdeletions: Challenges and opportunities for genotype/phenotype correlations in patients with large nf1 deletions. Genes (Basel) 12:. https://doi.org/10.3390/genes12101639
66. Serra G, Antona V, Corsello G, Zara F, Piro E, Falsaperla R (2019) NF1 microdeletion syndrome: Case report of two new patients. Ital J Pediatr 45:1–7. https://doi.org/10.1186/s13052-019-0718-7
67. Knorr DY, Hartung D, Schneider K, Hintz L, Pies HS, Heinrich R (2021) Locust Hemolymph Conveys Erythropoietin-Like Cytoprotection via Activation of the Cytokine Receptor CRLF3. Front Physiol 12:. https://doi.org/10.3389/fphys.2021.648245
68. Bonnas CB (2009) Identification of erythropoietin isoforms and evaluation of their biological importance.
69. Chong ZZ, Kang JQ, Maiese K (2003) Erythropoietin fosters both intrinsic and extrinsic neuronal protection through modulation of microglia, Akt1, Bad, and caspase-mediated pathways. Br J Pharmacol 138:1107–1118. https://doi.org/10.1038/sj.bjp.0705161
70. Siren A-L, Fratelli M, Brines M, Goemans C, Casagrande S, Lewczuk P, Keenan S, Gleiter C, Pasquali C, Capobianco A, Mennini T, Heumann R, Cerami A, Ehrenreich H, Ghezzi P (2001) Erythropoietin prevents neuronal apoptosis after cerebral ischemia and metabolic stress. Proc Natl Acad Sci 98:4044–4049. https://doi.org/10.1073/pnas.051606598
71. Weishaupt JH, Rohde G, Pölking E, Siren AL, Ehrenreich H, Bähr M (2004) Effect of erythropoietin axotomy-induced apoptosis in rat retinal ganglion cells. Investig Ophthalmol Vis Sci 45:1514–1522. https://doi.org/10.1167/iovs.03-1039
72. Wen TC, Sadamoto Y, Tanaka J, Zhu PX, Nakata K, Yong-Jie M, Hata R, Sakanaka M (2002) Erythropoietin protects neurons against chemical hypoxia and cerebral ischemic injury by up-regulating Bcl-xL expression. J Neurosci Res 67:795–803. https://doi.org/10.1002/jnr.10166
73. Cheng XY, Biswas S, Li J, Mao CJ, Chechneva O, Chen J, Li K, Li J, Zhang JR, Liu CF, Deng W Bin (2020) Human iPSCs derived astrocytes rescue rotenone-induced mitochondrial dysfunction and dopaminergic neurodegeneration in vitro by donating functional mitochondria. Transl Neurodegener 9:1–14. https://doi.org/10.1186/s40035-020-00190-6
74. Merelli A, Ramos AJ, Lazarowski A, Auzmendi J (2019) Convulsive Stress Mimics Brain Hypoxia and Promotes the P-Glycoprotein (P-gp) and Erythropoietin Receptor Overexpression. Recombinant Human Erythropoietin Effect on P-gp Activity. Front Neurosci 13:750. https://doi.org/10.3389/fnins.2019.00750
75. Chin K, Yu X, Beleslin-Cokic B, Liu C, Shen K, Mohrenweiser HW, Noguchi CT (2000) Production and processing of erythropoietin receptor transcripts in brain. Mol Brain Res 81:29–42. https://doi.org/10.1016/S0169-328X(00)00157-1
76. Chen AY, Guan W, Lou S, Liu Z, Kleiboeker S, Qiu J (2010) Role of Erythropoietin Receptor Signaling in Parvovirus B19 Replication in Human Erythroid Progenitor Cells. J Virol 84:12385–12396. https://doi.org/10.1128/JVI.01229-10

77. Cohrs G, Goerden S, Lucius R, Synowitz M, Mehdorn HM, Held-Feindt J, Knerlich-Lukoschus F (2018) Spatial and Cellular Expression Patterns of Erythropoietin-Receptor and Erythropoietin during a 42-Day Post-Lesional Time Course after Graded Thoracic Spinal Cord Impact Lesions in the Rat. J Neurotrauma 35:593–607. https://doi.org/10.1089/neu.2017.4981
78. Sanchez PE, Fares RP, Risso J, Bonnet C, Bouvard S, Morales A, Pequignot J, Baulieu E, Levine RA, Bezin L (2009) Optimal neuroprotection by erythropoietin requires elevated expression of its receptor in neurons. PNAS 106:1–6
79. Wakhloo D, Scharkowski F, Curto Y, Javed Butt U, Bansal V, Steixner-Kumar AA, Wüstefeld L, Rajput A, Arinrad S, Zillmann MR, Seelbach A, Hassouna I, Schneider K, Qadir Ibrahim A, Werner HB, Martens H, Miskowiak K, Wojcik SM, Bonn S, Nacher J, Nave KA, Ehrenreich H (2020) Functional hypoxia drives neuroplasticity and neurogenesis via brain erythropoietin. Nat Commun 11:1–12. https://doi.org/10.1038/s41467-020-15041-1
80. Yang C, Zhao T, Lin M, Zhao Z, Hu L, Jia Y, Xue Y, Xu M, Tang Q, Yang B, Rong R, Zhu T (2013) Helix B surface peptide administered after insult of ischemia reperfusion improved renal function, structure and apoptosis through beta common receptor/erythropoietin receptor and PI3K/Akt pathway in a murine model. Exp Biol Med 238:111–119. https://doi.org/10.1258/ebm.2012.012185
81. Xu X, Cao Z, Cao B, Li J, Guo L, Que L, Ha T, Chen Q, Li C, Li Y (2009) Carbamylated erythropoietin protects the myocardium from acute ischemia/reperfusion injury through a PI3K/Akt-dependent mechanism. Surgery 146:506–514. https://doi.org/10.1016/j.surg.2009.03.022
82. Persad R, Liu C, Wu T, Houlihan PS, Hamilton SR, Diehl AM, Rashid A (2004) Overexpression of caspase-3 in hepatocellular carcinomas. 861–867. https://doi.org/10.1038/modpathol.3800146
83. Naseri MH, Mahdavi M, Davoodi J, Tackallou SH (2015) Up regulation of Bax and down regulation of Bcl2 during 3-NC mediated apoptosis in human cancer cells. Cancer Cell Int 1–9. https://doi.org/10.1186/s12935-015-0204-2
84. He XIN, Sun J, Huang X (2018) Expression of caspase-3, Bax and Bcl-2 in hippocampus of rats with diabetes and subarachnoid hemorrhage. 873–877. https://doi.org/10.3892/etm.2017.5438
85. Hu X, Li Z, Lin R, Shan J, Yu Q, Wang R, Liao L, Yan W, Wang Z, Shang L, Huang1 Y, Zhang1 Q, Xiong K (2021) Guidelines for Regulated Cell Death Assays: A Systematic Summary, A Categorical Comparison, A Prospective. 9:1–28. https://doi.org/10.3389/fcell.2021.634690

Declarations

Funding

This work was supported by the Deutsche Forschungsgemeinschaft (DFG; Project number: 398214842 and 499371712).

Competing interests

The authors declare no competing interest.

Author Contributions

DYK, IRP, RB and RH designed and supervised the study. DYK, IPR ,HSP, SP, NSD performed experiments. DYK, IRP and HSP analysed the data. DYK, IRP and RH wrote the manuscript. All authors read and approved of the manuscript.

Data availability

The datasets generated during and/or analysed during the current study are available from the corresponding author on reasonable request.

Ethics approval

N/A

Consent to participate

N/A

Figures

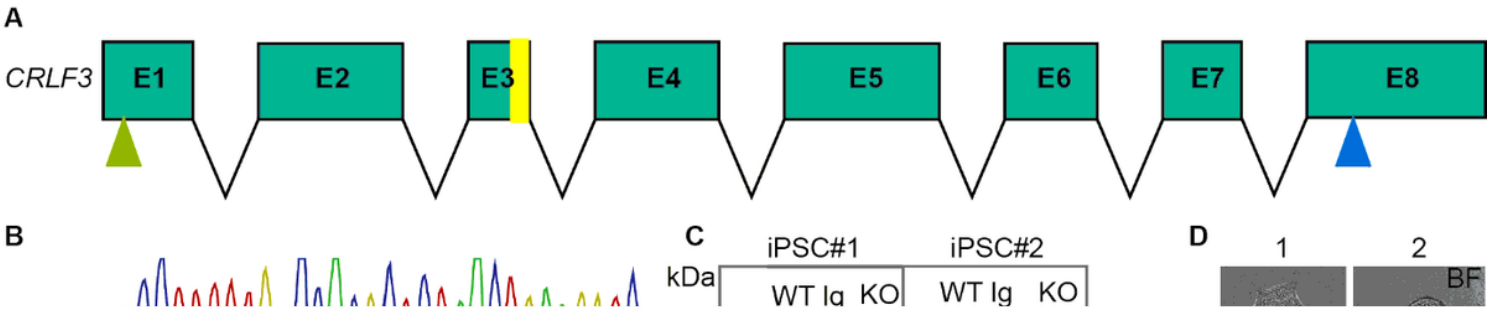

Figure 1

Characterization of CRISPR-induced CRLF3 mutation in human iPSC lines. **A:** Schematic overview of CRLF3 gene. Exons are represented as boxes, with sizes corresponding to exon length. Introns are represented as arrows and do not depict intron length. Yellow bar in exon 3 (E3) shows mutation site. Green and blue arrows mark start and stop codon of the coding sequence respectively. **B:** Chromatograms illustrating mutations in alleles A and B of iPSC#X line. Top: WT sequence, with gDNA scaffold marked by framed portion of the nucleotide sequence. Middle: Allele A of the mutated line, which is characterized by one deleted base pair (marked with arrow) and a base pair exchange (marked by red box). Bottom: Allele B of the same iPSC line lacking a row of 5 deleted base pairs. Both mutations induce frameshifts that generate premature stop codons. **C:** Western blot analysis of Ig-Ctrl and mutated iPSC lines and differentiated neurons. Top: Protein lysates of iPSC#1 and #2 probed for CRLF3 and αTubulin. WT and Ig-Ctrl lysates show bands for CRLF3 protein, while the mutated lines (marked with KO) do not. αTubulin probed as loading control appears for all lines. Bottom: Western blot analysis of differentiated neurons originating from WT or CRLF3 mutated cells of both lines. While WT lysates show bands for CRLF3, no protein was detected in KO cells. αTubulin bands are present. **D:** Transfected iPSC colonies express EGFP as reporter gene. Both lines show homogeneous eGFP expression within iPSC colonies consisting of more than 100 cells. Scale bar: 50 µM

Figure 2

ß-III-tubulin stainings of iPSC-derived neurons. **A:** Cells derived from iPSC#1. **B:** iPSC#2-derived neurons. All generated cell lines contain extensive axonal networks and anatomical cell-cell contacts. Scale bar 100 µM

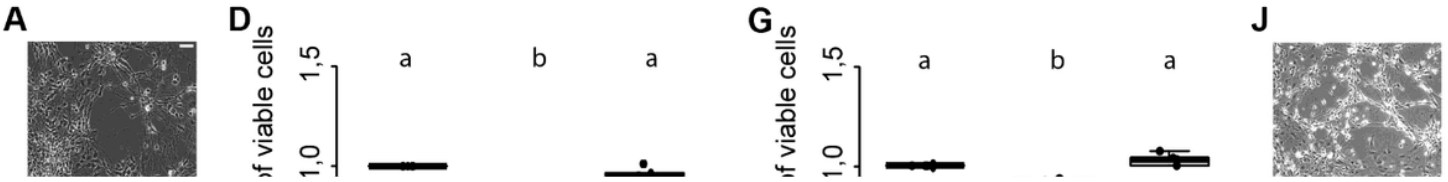

Figure 3

EV-3 induces CRLF3-mediated protection of human iPSC-derived neurons (left: iPSC#1; right: iPSC#2). Horizontal panels depict data and images from WT (A), isogenic controls (Ig-Ctrl) (B) and CRLF3-mutated (KO) (C) iPSC-derived neurons. **A, B, C, J, K, L:** Brightfield and fluorescent images of iPSC-derived neurons.

Ig-Ctrl (B) and KO (C) cells display GFP fluorescence, indicating Cas9-GFP fuse transcript. **D, E, F, G, H, I:** Relative survival of iPSC-derived neurons. Cells were prepared for FACS analysis by live/dead and ß-III-tubulin staining. **D, E, F:** Data collected for neuron-like cells originating from iPSC#1. 18 h exposure to 800 nM rotenone reduced the survival of WT (D), Ig-Ctrl (E) and KO (F) neurons significantly when normalized and compared to survival in respective untreated control cultures. Rotenone-induced cell death was prevented by EV-3 (41,5 ng/ml) in WT and Ig-Ctrl neurons but not in CRLF3- KO neurons. Numbers of analyzed neurons: WT 313.250, Ig-Ctrl 292.996, KO 129.191. n = 5 for all. **G, H, I:** Relative survival of iPSC-derived neurons originating from iPSC#2. Cells were prepared for FACS analysis by live/dead and ß-III-tubulin staining. 18 h exposure to 1 µM rotenone reduced the survival of WT (D), Ig-Ctrl (E) and KO (F) neurons significantly when normalized and compared to survival in respective untreated control cultures. Rotenone-induced cell death was prevented by EV-3 (33,3 ng/ml) in WT and Ig-Ctrl neurons but not in CRLF3- KO neurons. Treatment of Ig-Ctrl neurons to EV-3 significantly increased cell survival in comparison to control cells. Numbers of analyzed neurons: WT 234.135, Ig-Ctrl 298.864, KO 279.976. n = 5 for WT and KO experiments, n = 6 for Ig-Ctrl. Data is presented as boxplots showing the median cell survival, upper and lower quartile and whiskers representing 1,5 x interquartile ranges. Single data points are shown as circles within the boxplot. Statistics with pairwise permutation test and Benjamini-Hochberg correction for multiple comparison. Significant differences ($p<0,05$) are indicated by differing letters

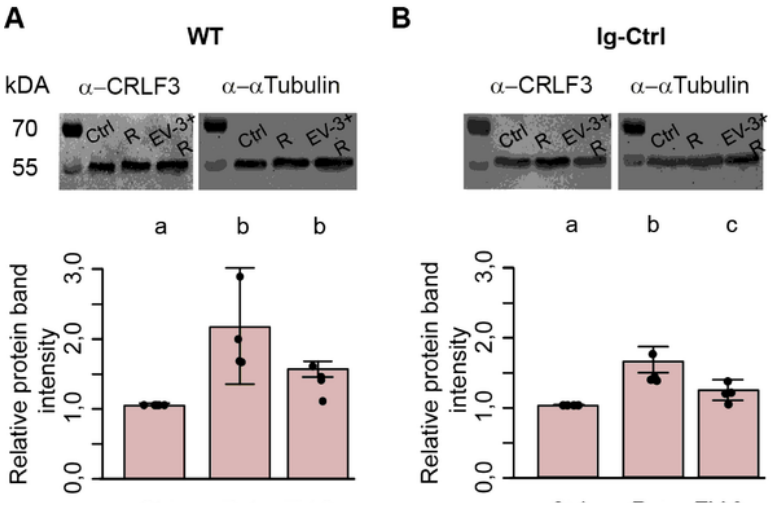

Figure 4

CRLF3 protein levels in apoptogenic and rescue conditions. Treatment with EV-3 and/or rotenone for 12 + 18 h started on day 30 of the differentiation protocol. Immediately after treatment, samples were collected. **A, B:** Protein immunoblots of iPSC#1-derived WT (A) and Ig-Ctrl (B) neurons labelled with anti-CRLF3 (left) and anti-αTubulin (right) as loading control. Both antibodies labelled single bands of the expected molecular size (both ~55 kDa) in each sample. Rotenone (800 nM) increased CRLF3 protein

levels in WT and Ig-Ctrl neurons. Co-treatment with EV-3 (41,5 ng/ml) reduced rotenone-induced CRLF3 accumulation insignificantly in WT and significantly in Ig-Ctrl neurons. n= 4. **C, D:** Protein immunoblots of iPSC#2-derived WT (A) and Ig-Ctrl (B) neurons labelled with anti-CRLF3 (left) and anti-αTubulin (right) as loading control. Both antibodies labelled single bands of the expected molecular size. Neither rotenone (1 µM) alone nor its combination with EV-3 (33,3 ng/ml) altered CRLF3 protein levels significantly. n= 3. Data is shown as bar plots representing the average band intensities measured together with the calculated standard deviation and single data points. Statistics: pairwise permutation test with Benjamini-Hochberg correction for multiple comparison. Significant differences ($p<0,05$) are indicated by differing letters. **E:** Immunofluorescent labeling of neurofilament 200 (NF200; neuronal/axonal marker) and CRLF3 in all iPSC#2-derived neurons. Nuclei were labelled with Dapi. CRLF3 immunoreactivity in WT and Ig-Ctrl covers entire neurons with extensive labelling in the soma. No CRLF3 imunoreactivity is detected in KO cells. Scale bars 100 µM

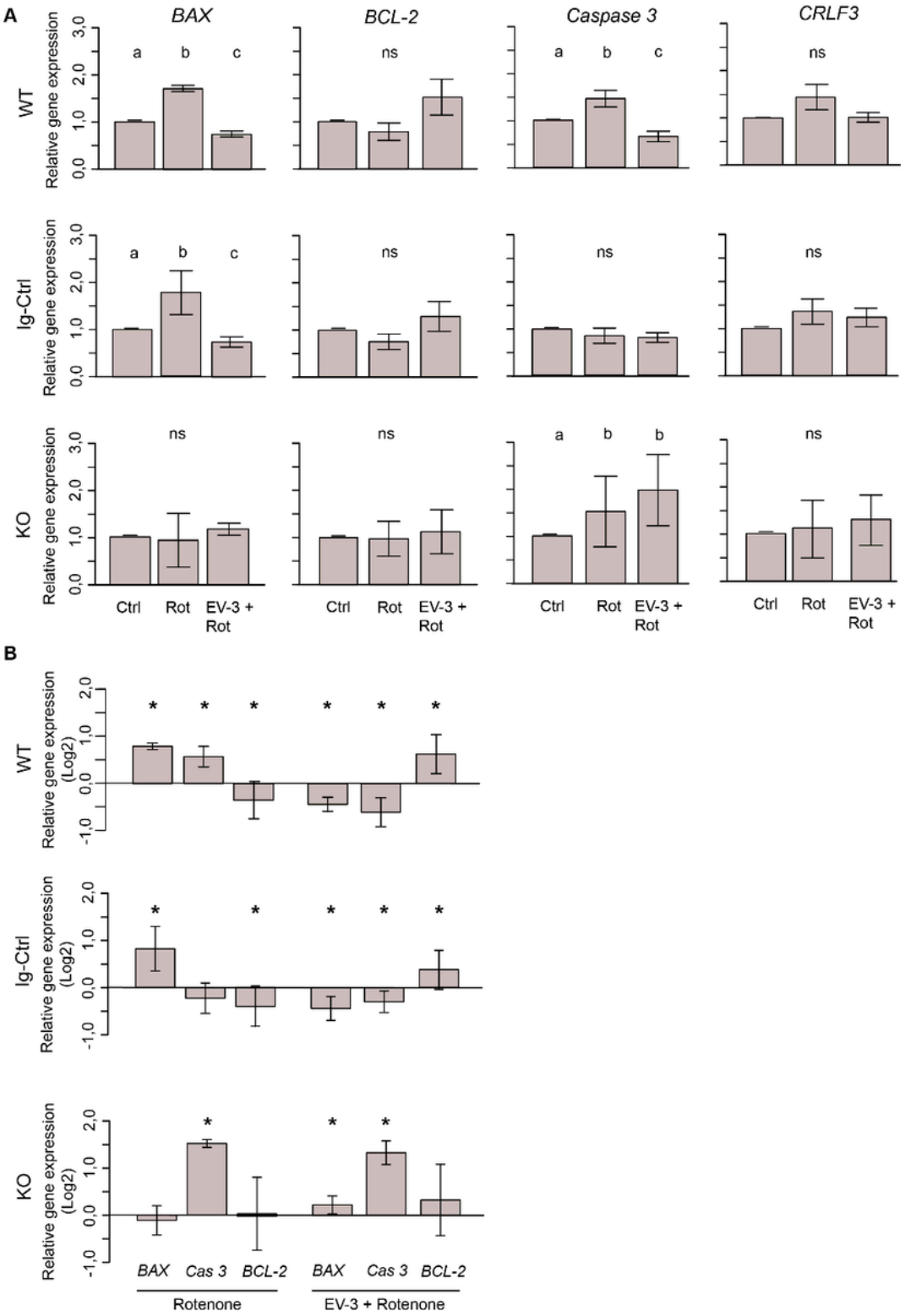

Figure 5

Expression of pro- and anti-apoptotic genes and *CRLF3* in iPSC#1-derived neurons. **A:** qPCR-based relative gene expression of pro-apoptotic *BAX* and *Caspase 3*, anti-apoptotic *BCL-2* and *CRLF3* in WT, Ig-Ctrl and CRLF3 KO lines after exposure to rotenone ± EV-3 (12 h EV-3 treatment, followed by 18 h rotenone exposure). Values were normalized to untreated controls. n=4 for each cell line. Graphics show average ± STDV; statistics with pairwise permutation test and Benjamini-Hochberg correction for multiple

comparison. Significant differences (p<0,05) are indicated by differing lettering. **B:** Same data as in (A) illustrated as log2 for direct comparison of GOI up- and down regulation between different treatments of WT, Ig-Ctrl and KO neurons. Relative gene expression in pharmacologically treated cultures were only compared to respective untreated controls. Graphics show average ± STDV; Statistics with t-test. Significant differences (p<0,05) are indicated by asterisk

Supplementary Files

This is a list of supplementary files associated with this preprint. Click to download.

- SupplementalInformation.docx